Hindawi
Advances in Materials Science and Engineering
Volume 2021, Article ID 5946148, 15 pages
https://doi.org/10.1155/2021/5946148

Research Article

Monitoring and Assessment of Cemented Paste Backfill Containing Coal Gangue and Fly Ash in an Underground Mine

Xinguo Zhang[1,2] **Jinhai Zhao**[1,2] **Lin Xin**[1,2] **Kun Wang**[1,2] **and Haiyang Pan**[1,2,3]

[1]*State Key Laboratory Breeding Base for Mining Disaster Prevention and Control, Shandong University of Science and Technology, Qingdao 266590, China*
[2]*College of Energy and Mining Engineering, Shandong University of Science and Technology, Qingdao 266590, China*
[3]*Exploration and Research Institute, China National Administration of Coal Geology, Beijing, China*

Correspondence should be addressed to Jinhai Zhao; jinhai.zhao@sdust.edu.cn and Haiyang Pan; phycumt@163.com

Received 27 March 2020; Revised 30 January 2021; Accepted 30 January 2021; Published 23 February 2021

Academic Editor: Shengwen Tang

Cemented coal gangue paste backfill (CCGPB) containing coal gangue and fly ash is a backfilling technique newly developed in coal mines in China that allows environmentally hazardous products, such as gangue and fly ash, to be reused in underground stopes. CCGPB materials provide efficient ground support for the caving of strata and reduce surface subsidence. In this paper, field monitoring of CCGPB properties was conducted in an underground coal mine, which mainly included the measurement of the longwall face temperature, humidity, CCGPB internal hydration temperature, stress conditions inside the backfills, and displacement. First, the components of the backfills, paste technique, slurry generation procedures, coalfield geology, and mining conditions were introduced. Then, a monitoring system was designed in the field. An online monitoring system was installed. The results of the field monitoring showed that the curing temperature significantly varied, i.e., from 26°C near the main gate to 37°C near the tailgate. The curing humidity had the same trends, increasing from 60% relative humidity (RH) near the main gate to 81% RH near the tailgate. The internal hydration process of the paste was divided into four stages, i.e., the rapid hydration stage, slower hydration stage, rapid decline hydration stage, and relatively stable stage. The highest hydration temperature was 50°C, which was measured on the second day after the backfill process. The temperature approached stability at 41°C. The evolution of the roof stress applied on the CCGPB was divided into four stages: the development stage, regulation stage, rapid growth stage, and relatively stable stage. The maximum roof loading was 12 MPa in the middle of the longwall face. The deformation of the backfill experienced four stages, i.e., the rapid deformation stage, slow deformation stage, relatively stable stage, and long-term stable stage. The maximum deformation was 104.3 mm, appearing in the middle of the face. In addition, the compression ratio of the backfill was approximately 4%. The results of this study showed that the working conditions of backfills in the field were different from those in the laboratory. This paper provides guidance for the design of the CCGPB technique and the predictions of surface subsidence induced by the production process of underground mining.

1. Introduction

Cemented coal gangue paste backfill (CCGPB) containing coal gangue and fly ash is an emerging backfill technique in coal mines in China. CCGPB not only disposes solid waste (mainly coal gangue and fly ash generated from coal cleaning plants and coal-fired power plants) but also significantly improves the recovery ratio of coal resources [1, 2]. As a type of cement-based mixture, CCGPB is mainly composed of coal gangue, fly ash, cement, and water [3–5]. Generally, CCGPB is produced in a surface preparation plant and delivered to the underground stope by pipeline through either gravity force or pumping force. Due to the good management of ground surface subsidence, the high recovery ratio of coal or ore, and the effective disposal of solid waste, the development of CCGPB is important for the green mining of coal resources in China [6–9].

In general, the technique of preparing CCGPB in the laboratory is determined by the uniaxial compressive

strength (UCS) of samples. Based on standard GB/T50081 in China, the laboratory curing conditions are set as follows: temperature of $20 \pm 2^{\circ}C$ and humidity of ≥95%. Concrete or CCGPB specimens are prepared in a standard curing chamber, and the curing time is set to 28 days [10, 11]. However, some studies have shown that the field conditions significantly affect the hardening process and the strength development of CCGPB [12, 13]. Based on these studies, a proper high temperature can accelerate the hydration progress and contribute to strength development, while a relatively lower temperature (the temperature below $0^{\circ}C$) is unfavorable for the hydration reaction. However, an overly high temperature can induce crack initiation in the backfills, which affects the mechanical properties and causes the CCGPB to have low strength. Since CCGPB is also a cement-based material, it is necessary to illustrate the effect of temperature on CCGPB strength in the underground environment. Another important factor in the strength of CCGPB is humidity. Some studies have shown that humidity is very important [13–15]. When the relative humidity is less than 80%, the hydration reaction tends to nearly stop. On the other hand, in the early curing process, without adequate humidity, a large amount of water is evaporated, which not only has a large impact on the hydration reaction but also leads to dry shrinkage on the surface of CCGPB. Due to the effect of dry shrinkage, tensile stress is generated on the surface of CCGPB, and then cracks are generated. As a result, the ultimate strength of CCGPB decreases [16]. Another important factor that affects CCGPB is the curing time. Generally, the curing time is determined by the type of binder agent and the release rate of hydration heat [16] investigated the effect of curing time on the one-dimensional consolidation behavior of CCGPB that contained different types and contents of cement using an improved lab apparatus. Some empirical equations were proposed in this study. Cao and Song [17] conducted an experiment to study the effect of interval time on the uniaxial compressive strength. In addition, other studies on the compressive strength, including different specimen sizes [18], solid components [19], binder types [20, 21], and microstructures [22–24], were conducted.

At present, in most of these studies, conventional molds were used under standard curing conditions in the laboratory, while field stress conditions were not considered. In only a few studies, the field curing conditions were mimicked in laboratories, and the effects of these conditions on the mechanical properties were analyzed [25]. Some studies indicated that for the same CCGPB techniques, the UCS of CCGPB prepared in the field was usually 2–4 times higher than that in the laboratory [26–30]. The difference was due to the consolidation environment of CCGPB in the field increasing the strength development and the ultimate strength. However, field experience showed that it is very difficult to replicate a real underground consolidation environment. Moreover, field curing conditions vary greatly when the paste placement method and the mining environment change. Therefore, only a few studies have been conducted underground in the field. To obtain the strength of CCGPB in the field, it is very important to test in both intrinsic and extrinsic curing environments. In this paper, field monitoring was used to investigate the impacts of field curing and stress environment on the properties of CCGPB.

2. Materials and Backfilling Methods

2.1. Characteristics of Components

2.1.1. Coal Gangue. The coal gangue used in this study was obtained from the crushing plant of a coal mine located in Jining, Shandong Province, China. To meet the requirements of pipeline delivery, the maximum particle size of the coal gangue was smaller than 25 mm [31], which is significantly different from the size of tailing particles (<2 mm). The main reason for the size of the coal gangue is the power required for crushing coal gangue. As shown in Figure 1, the raw gangue had a large particle size, i.e., approximately 300 mm. The power required for crushing the coal gangue from a particle size of 300 mm to 25 mm was much lower than that required for crushing the coal gangue to a particle size below 2 mm. The second reason for the size of the gangue is that an artificial separating wall, which is an important backfilling process, can relatively easily contain slurries containing larger particles. The purpose of installing an artificial separating wall is to prevent slurry leakage. Additionally, some studies have shown that CCGPB slurry containing large particles has good liquidity and ultimate hardening strength [32]. To meet the transportation requirements for slurry, the content of the finer particles should be higher than 40% [33] because finer particles contain more water and can be easily transported by a pipeline system. Therefore, a specially designed jaw crusher was used to crush the coal gangue. In addition, two stages of crushing were needed before the coal gangue particle size reached the required size range (<25 mm) [34, 35]. In the first stage, the coal gangue was crushed from the maximum particle size of 300 mm to 50 mm. In the second stage, the product from the first stage was processed by a finer crusher, and particles with sizes below 25 mm were obtained, as shown in Figure 2. After crushing, the coal gangue was processed by a series of graded sieves to meet the requirement for the distribution of the particle size [36–38], as shown in Figure 3. It can be seen that after the two-stage process, 54% of the coal gangue was in the form of particles with small size (<5 mm), while particles sized larger than 10 mm accounted for only approximately 22 wt%. Thus, most of the particles were sized in the range between 0.1 mm and 10 mm, which was suitable for the production of CCGPB materials. The chemical composition of the coal gangue was another important factor that needed to be considered. For coal gangues with high contents of montmorillonite and illite, muddy hydration occurs when these minerals encounter water [12, 13, 39]. As a result, the viscosity of the slurry is increased by these minerals, and serious blockages can occur in transporting pipelines. The chemical composition of the coal gangue was analyzed by X-ray diffraction and is summarized in Table 1. The content

Figure 1: Raw coal gangue.

Figure 2: Coal gangue after the second crushing.

of SiO_2 accounted for 51.92% of the weight. Therefore, the coal gangue used in this study was suitable for the production of CCGPB materials.

2.1.2. Hydraulic Binder. In this study, to increase the workability and pumpability of the paste slurry, ordinary Portland cement (OPC) was used as the hydraulic binder, and fly ash was used as an additive [40, 41]. From the analysis of the particle size of the coal gangue, the average particle size of the coal gangue was larger than that of tailings. Fly ash can be used as a finer aggregate to reduce the total average particle size and avoid blockage of pipelines. Additionally, due to the cementitious capabilities and the low price of fly ash, the usage of fly ash can reduce the consumption of OPC and reduce the cost of the backfilling material [12, 13, 31]. The fly ash used in this study was collected from a coal-fired power plant near the coal mine. The chemical composition of the fly ash is summarized in Table 1. The content of CaO accounted for 15.13% of the total weight of the fly ash; thus, the fly ash was of type C. A laser particle analyzer (DVM5000HD) and SEM imaging technology were used to investigate the distribution of the particle size, as shown in Figures 4 and 5. It can be observed that the fly ash had a small particle size and a higher content of spherical particles, which had a lubrication effect on pipeline transport. The finer content (<41 μm) in the fly ash was approximately 50%. The particle size of the fly ash was almost three orders of magnitude smaller than that of the coal gangue [42]. The water drainage ability and strength could be affected by the fineness of the particles. Therefore, an appropriate ratio between fly ash and coal gangue was required to optimize the workability of the paste and the strength of the CCGPB. In addition, the mixing water in the field was obtained from the municipal tap in the surface preparation plant.

2.2. Field Preparation of CCGPB. The technique used for the CCGPB was determined in the laboratory. According to the proportion tests in the lab, the ratio of coal gangue, fly ash, cement, and water was 7 : 1 : 1 : 4, and the mass concentration was 74% in the field. The particle of cement ranges from 10 μm to 80 μm, and the strength is 32.5 MPa. Its 3-day and 28-day compressive strengths are 30 MPa and 42.5 MPa, respectively. The preparation process of CCGPB mainly included a coal gangue crushing and warehousing system, an automatic feeding and mixing system, a pumping and pipeline delivering system, and a face separating and backfilling system, as shown in Figure 6.

2.3. Monitoring Procedures

2.3.1. Monitoring Scheme. In this paper, the field curing conditions mainly included the temperature and humidity of the working face. To understand the internal speed of hydration of CCGPB with underground curing age, the hydration temperature of the CCGPB was monitored. The stress conditions mainly included roof stress and displacement [43, 44]. In the field monitoring scheme, the geological conditions, the function of the monitoring instrument, the monitoring precision, and the blind spot region were considered. In particular, there was a high correlation between the geometric dimensions of the stope and the movement of the overlying strata. According to the thumb rule, the largest roof subsidence displacement occurs at the center of a mined-out region. Therefore, the monitoring stations should mainly cover the central region in a fully mechanized backfilling face. Three rows of monitoring sensors were installed, as shown in Figure 7. Sensors for hydration temperature, stress meters, and displacement meters were installed in the backfills. Sensors for curing temperature and humidity were installed in the working face. In the advancing direction of the face, three row lines were set up at intervals of 50 m. Each monitoring line was then subdivided into three zones with intervals of 25 m along the face-dip direction. A set of online monitoring systems was installed in the goaf region. The fresh air of the face was from the tail entry, and the exhaust air was discharged by the head entry after cleaning the face.

2.3.2. Monitoring System. The online monitoring system, which was specially developed by the Special Mining Institute of Shandong University of Science and Technology, included surface and underground units [43, 45–50]. The main instruments consisted of data acquisition equipment, transmission signal cables, communication monitoring substations, communication monitoring hosts, and

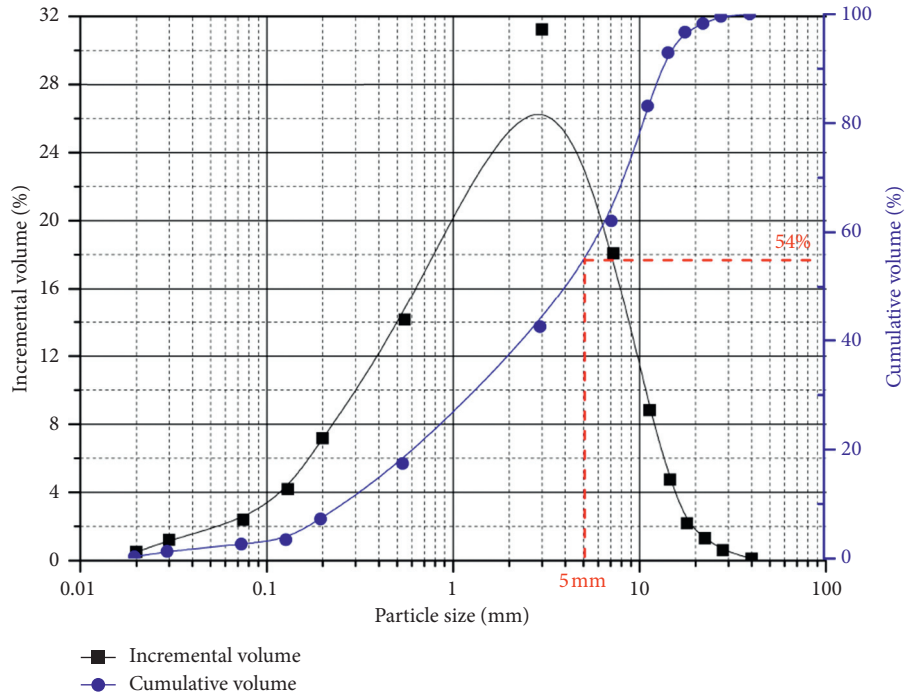

Figure 3: Particle size distribution of coal gangue.

Table 1: Chemical composition of coal gangue and fly ash.

Classification	Composition	Loss	SiO_2	Fe_2O_3	Al_2O_3	CaO	MgO	TiO_2	Na_2O	K_2O
Gangue	Percentage	17.8	51.92	3.87	19.03	1.0	1.18	0.75	0.54	1.47
Fly ash	Percentage	10.33	43.84	27.40	4.01	12.13	1.09	—	—	—

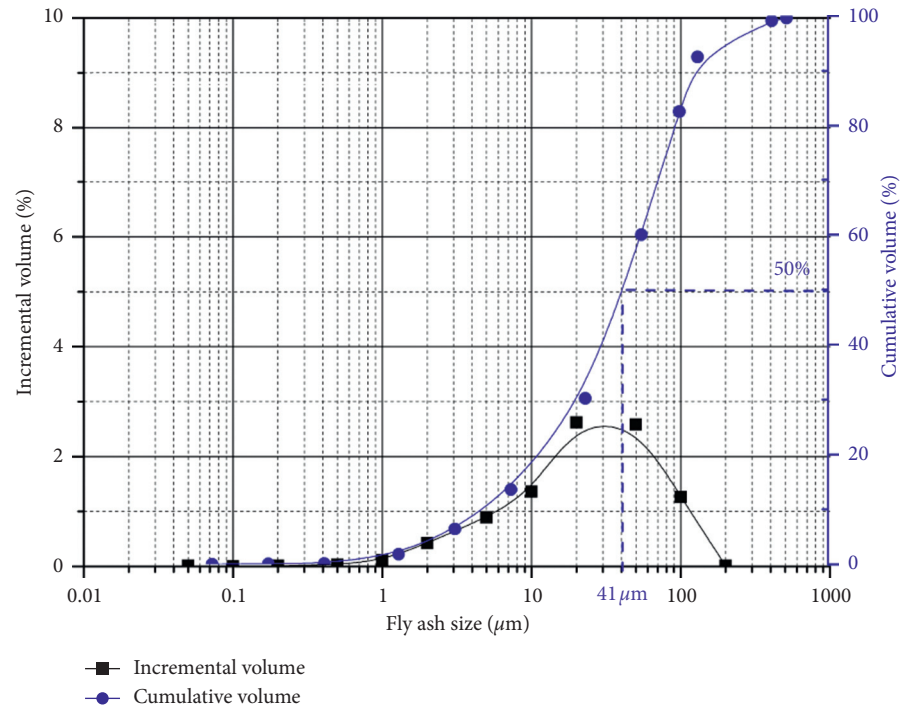

Figure 4: Particle size distribution of fly ash.

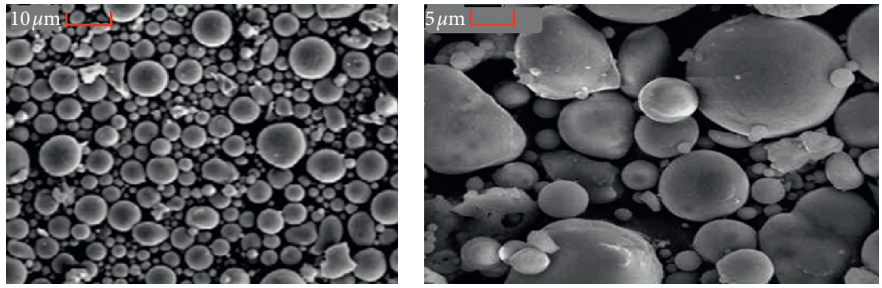

(a) (b)

Figure 5: SEM images of fly ash at different magnifications: (a) 10 μm scale and (b) 5 μm scale.

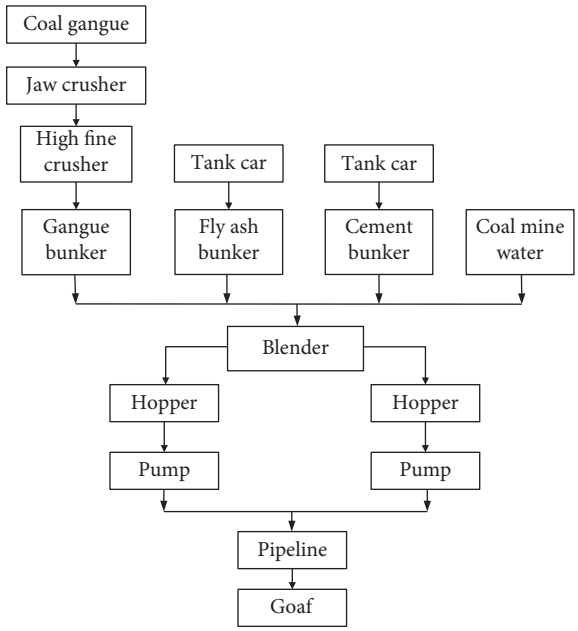

Figure 6: Field preparation process of CCGPB.

computers, as shown in Figure 8. The surface unit was connected with Industrial Ethernet through the monitoring host.

The parameters for the temperature and humidity sensors, hydration temperature sensor, stress meter, and displacement meter of the CCGPB are shown in Table 2.

A DHT11 digital temperature and humidity sensor was used to monitor the temperature and humidity of the working face. A DS18B20 digital temperature sensor was used to monitor the internal hydration temperature of the CCGPB. Based on the strain measuring technique, the CCGPB vertical stress was measured using a stress meter placed in the backfill. The mechanism was activated when the working face was advanced and the roof pressure was gradually applied to the backfill.

The stress meters were installed on the floor, as shown in Figure 9(b). Before the stress meters were installed, the floor was cleaned, and the output signal cables were sequentially labeled. Then, the stress meters were fastened to the circular steel plate with a clamping screw. Subsequently, the steel plate was fixed to the floor. All the interfaces need to be filled with glues to prevent water from entering.

A column-type displacement meter was used to monitor the deformation of the backfill. Resistance transducer technology was used in the measurement of displacement, as shown in Figure 10(a). When the CCGPB was gradually compressed by the overlying strata, the inner cylinder assembly was compressed, which drove the potentiometer to rotate. Then, a linear output voltage signal was generated with the change in the potentiometer. The voltage signal was then transmitted to communicate with the superior substation through RS485 communication.

3. Field Application

3.1. Geological Conditions. The study was conducted in an underground coal mine located in Jining, Shandong Province, China, which had a high coal reserve ratio of 80% under the village. The fully mechanized backfill technology mining method was adopted to extract a coal seam at a depth of approximately 500 m. The coal seam was approximately 2.7 m thick and dipped at an angle of approximately 12° toward the east. The width of the longwall working face and the length of the longwall panel were 100 m and 1100 m, respectively. There were goaves on both sides of the panel that were caved in previous longwall panels. At the time of this study, there were a total of 49 residual strip coal pillars in this mine, and the total recyclable coal reserves were as high as 10 million tons. There was a gangue dump with a total accumulation of more than 2 million tons and a thermal power plant that produced fly ash in amounts as high as 200 thousand tons annually. To recycle the residual coal pillars and dispose of the solid waste, fully mechanized CCGPB technology was applied in 2351 faces. Photographs of this technology in the field are shown in Figure 11.

3.2. Layout of the Monitoring System. In the field, a displacement meter, stress meter, and temperature sensor were used to monitor the stress and hydration conditions. The temperature and humidity sensors were used to monitor the face curing conditions. The layout of the field is shown in Figure 12. First, the sensors were connected to the communication substation in the air-return roadway. Then, the communication cable was connected to the central switch of the master communication. The cable was incorporated into Industrial Ethernet, and the collected data were transmitted

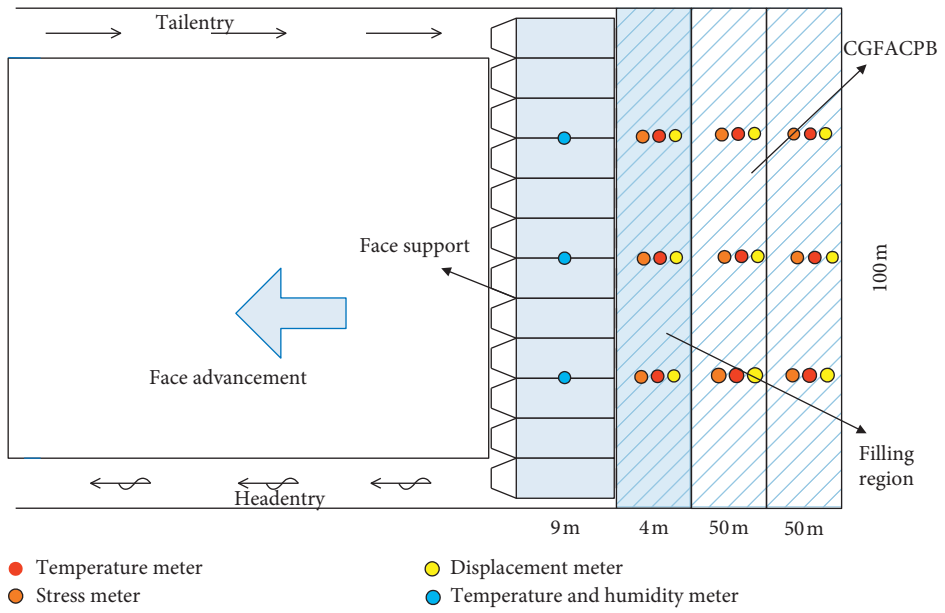

Figure 7: Monitoring scheme.

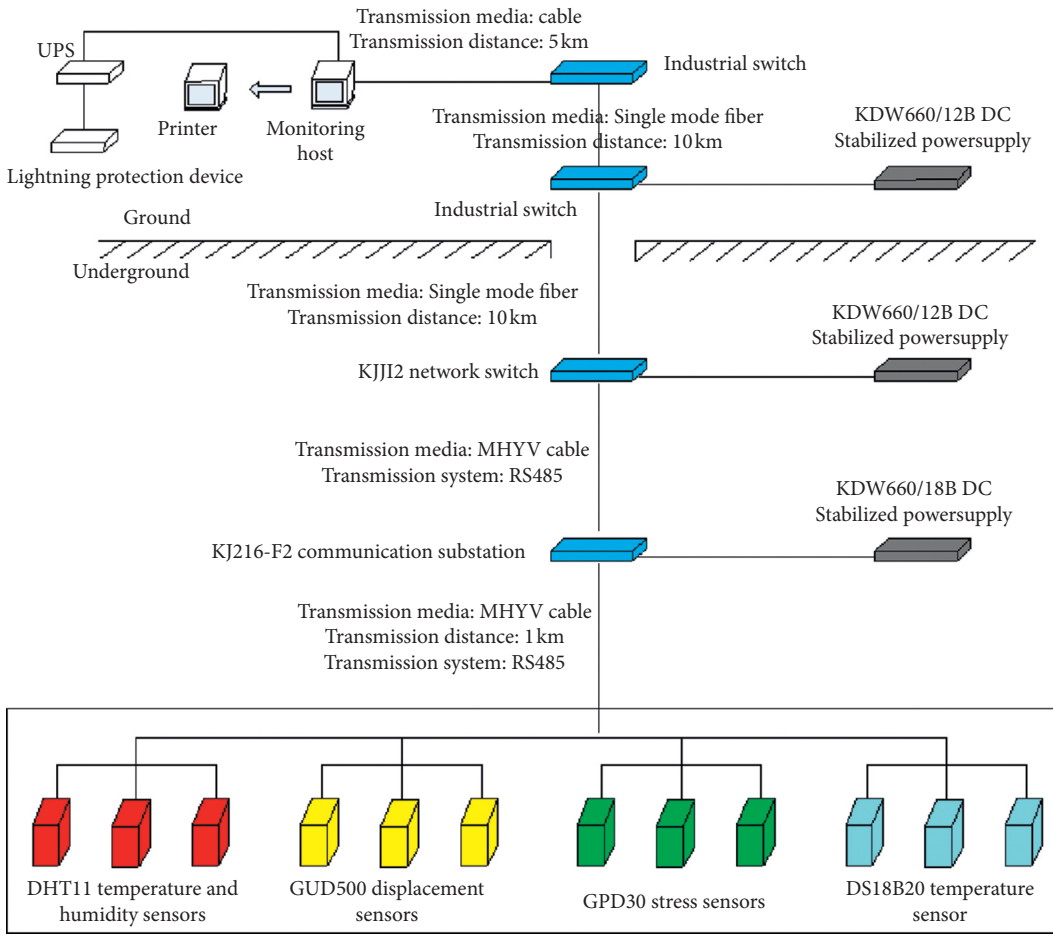

Figure 8: The online monitoring system.

Table 2: Parameters of sensors.

Sensor type	Parameters	Figures of sensors
Temperature and humidity sensors	Working voltage: 3–5 V; temperature measurement range: 0°C–50°C; humidity measurement range: 20–100%RH; temperature measurement accuracy 1°C; humidity measurement accuracy: 1% RH; transmission system RS485; transmission maximum distance: 1.2 km	
Hydration temperature sensor	Working voltage: 3–5 V; temperature measurement range: −55°C–+125°C; temperature measurement accuracy: ±0.5°C; transmission system: RS485; transmission maximum distance: 1.2 km	
Stress meter	Working voltage DC 18 V; working current:≤20 mA; transmission system: RS485; the cross-sectional area of transmission cables: 0.43 mm^2; transmission maximum distance: 1 km; measuring span 0–30 MPa; measuring error: ≤4.0% (FS); main dimension: φ118∗60.5 mm	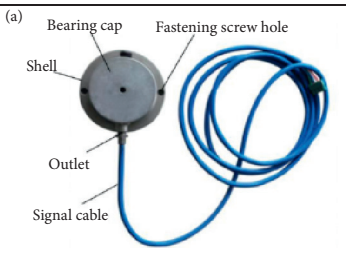
Displacement meter of CCGPB	Parameters: setting; working voltage: DC 18 V; working current: ≤20 mA; transmission system: RS485; cross-sectional area of transmission cables: 0.43 mm^2; transmission maximum distance: 1 km; measuring span: 0–500 mm; measuring error: ≤4.0% (FS); main dimension: φ186∗3000 mm	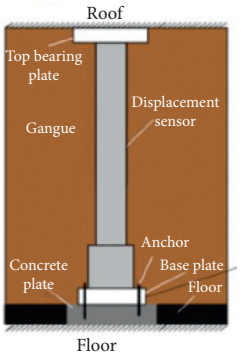

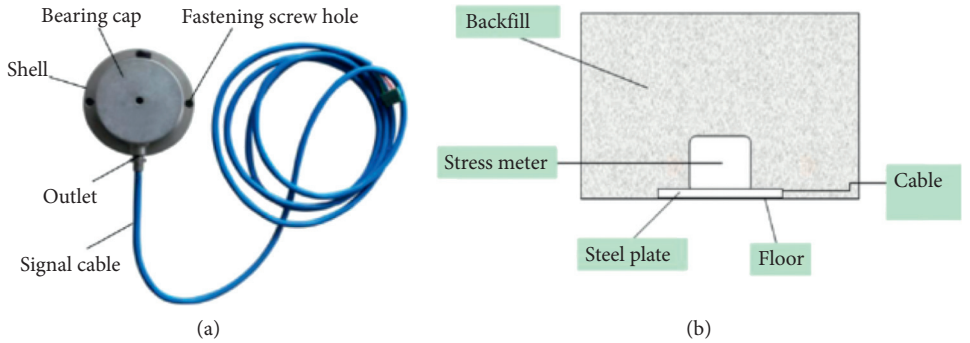

Figure 9: (a) Stress meters and (b) installation method.

to the ground monitoring host. The recording duration of the data was 5 s. In addition, the displacement, stress, temperature, and humidity were preset to 500 mm, 30 MPa, 125°C, and 100, respectively.

4. Results

4.1. Face Temperature and Humidity. The installation locations were divided into three sections, i.e., the upper, middle,

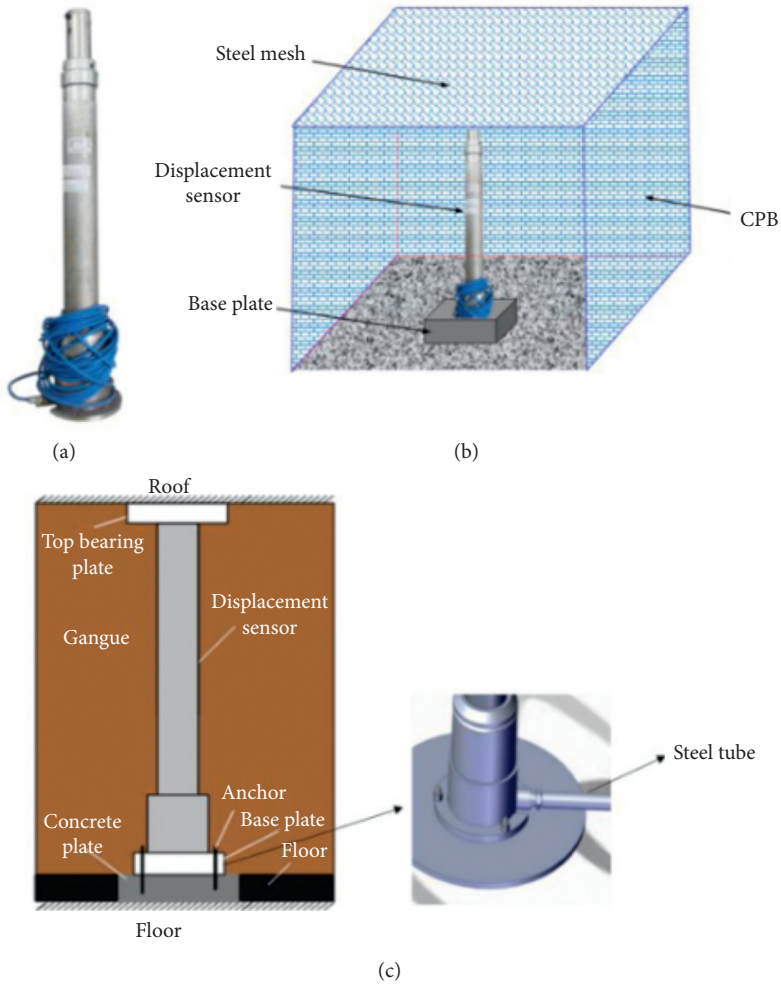

Figure 10: (a) Column-type displacement sensor, (b) installation of displacement sensor, and (c) components of the installed column-type displacement sensor.

and lower parts in the face. The position of the upper part was approximately 25 m from the tail entry, where there was a good ventilation environment and fresh air could enter. The middle part was located in the middle of the face, where there was a relatively good ventilation environment. The lower position was close to the head entry. After the face was washed with fresh air, the polluted air was discharged through the head entry [51–53]. The ventilation environment in the low position was very poor. Figures 13 and 14 show the changes in the temperature and humidity at different positions of the face within the backfill process.

Figures 13 and 14 show the temperature and humidity change of the face. The temperature of the upper face was in the range of 26°C–28°C. At the upper face, the speed of the airflow was relatively stable, and the temperature only slightly changed. Due to the large amount of fresh air consumed by equipment and personnel, the temperature at the middle face moderately changed, from the lowest value of 29.5°C to the highest value of 32°C. At the lower position close to the head entry, the temperature greatly changed, from the lowest of 34°C to the highest of 37°C. The humidity of the upper face was in the range of 60% to 62% RH, which was relatively comfortable. The humidity at the middle position was significantly higher, i.e., in the range of 70% to 73% RH. Workers might feel very damp in such high humidity. At the lower face, the humidity was in the range of 78% to 81% RH, which caused this area to be very unfit for personnel to work in.

4.2. Internal Hydration Temperature of Paste. CCGPB is a cement matrix material. The hydration of Portland cement is a very complicated and heterogeneous polyphase chemical reaction process. After the water is added, the hydration reaction occurs, in which the cement material structure gradually evolves and the state gradually changes from liquid to solid. Hydration heat refers to the heat released by the combination of matter and binder. When the concrete sets and hardens, heat is produced by the reactions between a variety of substances and water. Hydration is a long process and always releases heat. The amount of released heat may reflect the increase in the strength. Figure 15 shows the change in the hydration temperature at different positions in the face. Based on the temperature, the hydration process can be divided into four stages:

Figure 11: Photographs of the fully mechanized CCGPB technology in the field. (a) Paste preparation plant. (b) Field paste. (c) Backfilling region. (d) Artificial isolation.

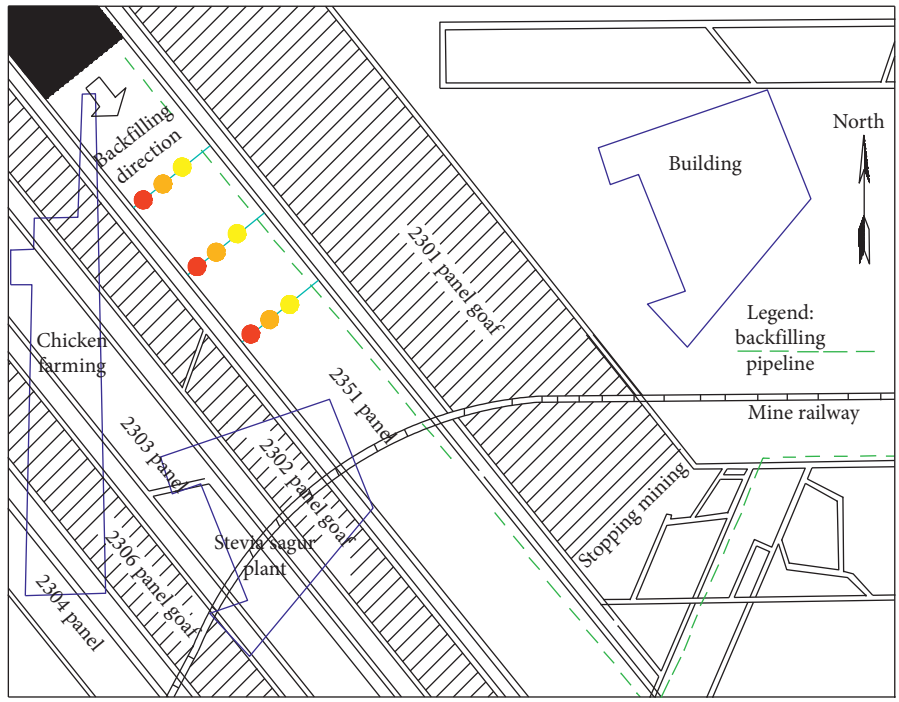

Figure 12: The field layout of the monitoring system.

(1) Rapid hydration stage: due to the differences in the ventilation conditions in the face and the heat released from personnel and equipment in different areas, there was a small gap in the temperature at different positions. The maximum hydration temperature, 50°C, was measured in the lower face,

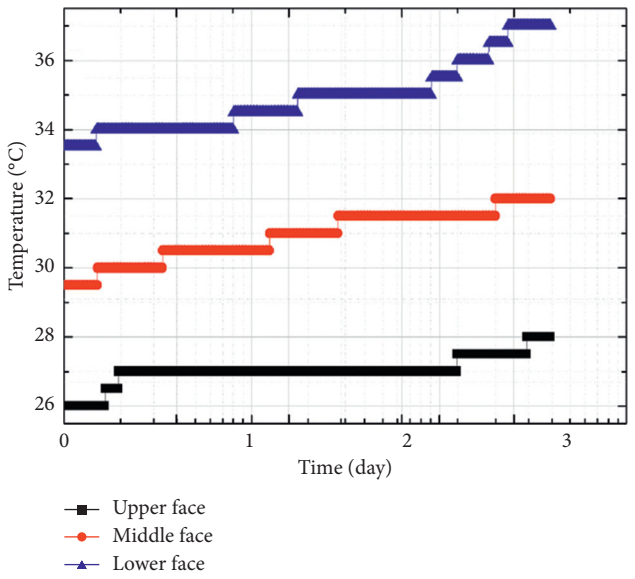

Figure 13: Temperature changes.

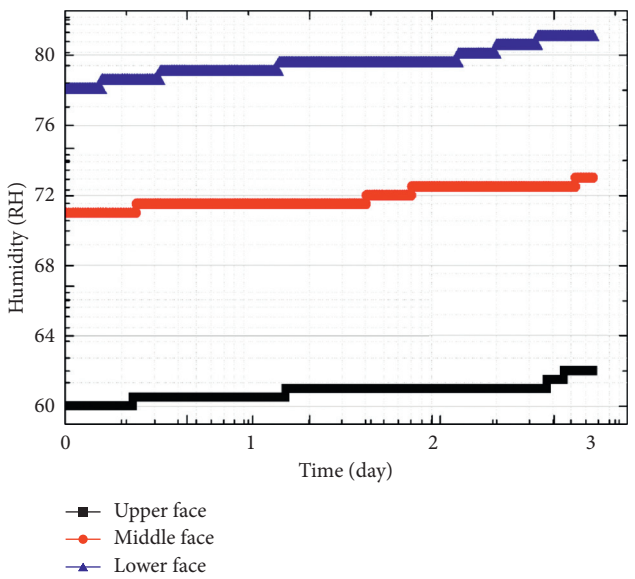

Figure 14: Humidity changes.

where the ventilation conditions were poor. The hydration reaction was strong for the first three days, especially on the second day. There was a slight decrease in the speed of the hydration reaction on the third day

(2) Slower hydration stage: this stage lasted for approximately 7 days, in which the temperature was kept stable not only in the middle of the face but also on both sides of the face. The temperature decreased by approximately 2°C at all positions of the face

(3) Rapid descending stage: this stage lasted for approximately 15 days, in which the temperature continued to decrease. After 24 days, the hydration temperature decreased from 47°C to 41°C in the upper face, from 48°C to 41.5°C in the middle face, and from 50°C to 42°C in the lower face

(4) Relatively stable stage: in this stage, the hydration temperature was kept basically stable not only in the middle of the face but also on both sides of the face. The conditions of temperature, humidity, and released heat were kept constant in all the areas. The temperature was 41°C at the upper and middle positions and 42°C at the lower position

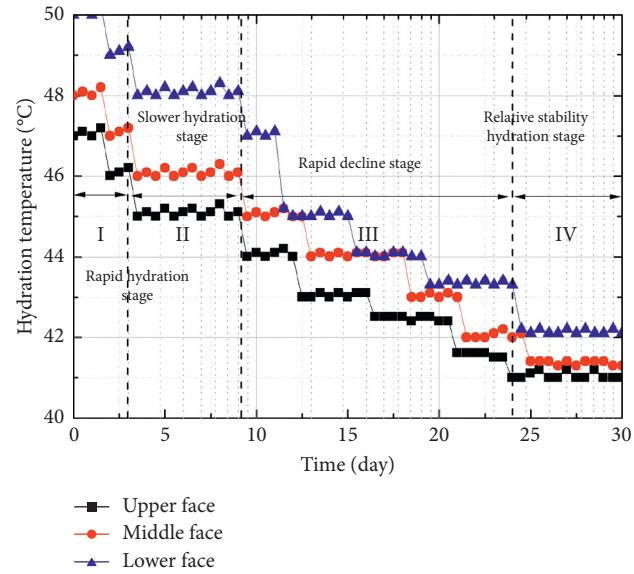

Figure 15: Trends of hydration temperature at different positions in the face.

4.3. Roof Loading. When the face was advanced from 180 m to 375 m, the development of the roof stress applied on the backfill is shown in Figure 16. The change in stress can be divided into four stages:

(1) Development stage: in this stage, the stress increased linearly from 0 MPa to 3.5 MPa as the face was advanced from 180 m to 240 m. The development of stress was rapid. Generally, the movement of the roof strata slowly caused the stress in the backfilling stope due to the limited movement space, and the number of involved strata increased. The concept of "three zones", i.e., the caving zone, fissure zone, and slow subsidence zone in the caved mining face, was not triggered. Therefore, in this stage, the stress developed due to the movement of the overlying strata

(2) Regulation stage: the stress applied on the backfill increased slowly from 3.5 MPa to 4 MPa as the face was advanced from 240 m to 270 m. The change in stress was relatively stable. Therefore, in this stage, the stress of the overlying strata was adjusted

(3) Rapid growth stage: in this stage, the stress applied on the backfill increased rapidly from 4 MPa to 11.5 MPa in the middle and from 3.5 MPa to 10 MPa on both sides as the face was advanced from 265 m to

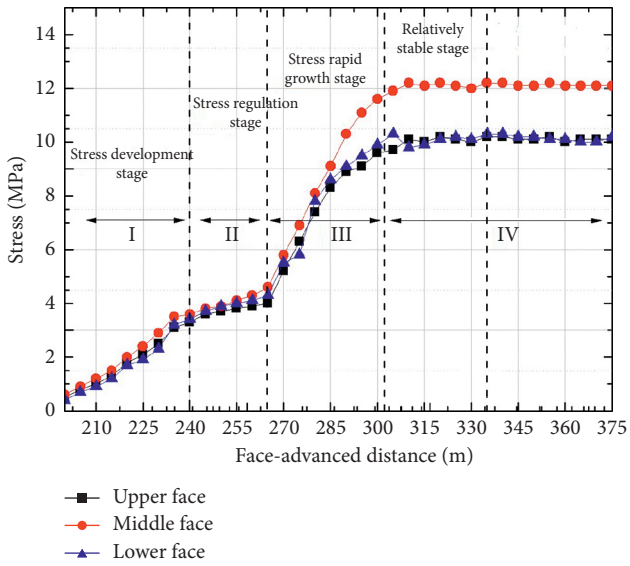

Figure 16: Trends of the stress of CCGPB with the advance of the face.

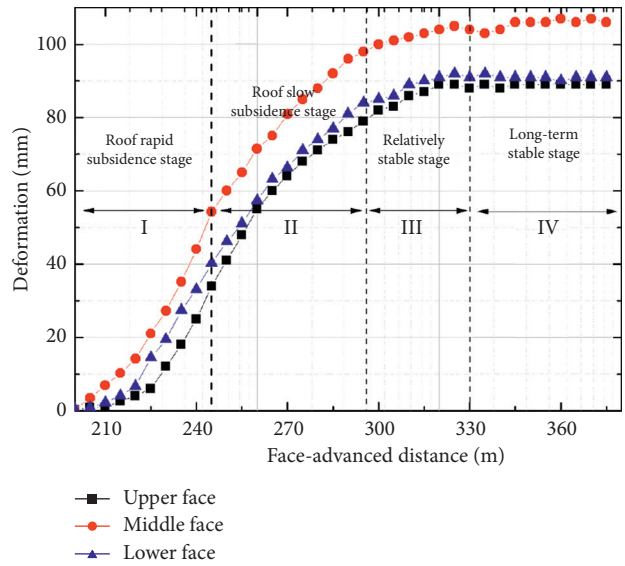

Figure 17: Trends of roof subsidence with the advance of the face.

300 m. In this stage, the face was pushed forward by approximately 105 m. The maximum value of stress was observed not only in the middle of the face but also on both sides of the face, which indicated that the whole overlying strata were applied on the backfill. In this stage, the stress of the overlying strata rapidly increased

(4) Relatively stable stage: the stress applied on the backfill increased slowly from 11.5 MPa to 12 MPa in the middle and from 10 MPa to 10.5 MPa on both sides. In this stage, the stress of the overlying strata was relatively stable. The stress applied on the backfill was relatively stable not only in the middle of the face but also on both sides of the face. A long-term stable trend can be observed from the change curve, which indicated that the whole overlying strata were stable

4.4. Roof Displacement. The main purpose of backfilling is to control overlying movement and prevent surface subsidence, as well as simultaneously dispose of solid waste and improve the resource recovery ratio. The factors affecting the surface subsidence included the immediate roof subsidence amount, the unconnected roof amount, the backfill compression amount, and the floor heaving amount [38, 54, 55]. The most important factor was the compression amount of paste backfill, which determined the level of surface subsidence. Figure 17 shows the cumulative roof displacement with the advance of the face. The roof's maximum displacement was 104.3 mm in the middle of the face. The trend of roof subsidence can be divided into four stages:

(1) Rapid subsidence stage: in this stage, the roof subsidence was 55 mm when the face was advanced from 180 m to 242 m. In addition, approximately 53% of the cumulative deformation occurred in the middle of the face. The rapid subsidence may have been caused by the relatively low initial strength of the CCGPB

(2) Slow subsidence stage: in this stage, the accumulative value of roof subsidence was approximately 40 mm, and approximately 38% of the cumulative deformation occurred in the middle of the face. Compared to Stage 1, i.e., the rapid subsidence stage, the subsidence significantly slowed with the advance of the face. According to related monitoring data, significant movement of the overlying strata occurred in this stage

(3) Relatively stable stage: in this stage, the cumulative roof subsidence was 11.3 mm, and the compression ratio of CCGPB was approximately 10% when the face was pushed forward to 140 m. This value showed that the roof was relatively stable and the amount of roof subsidence was obviously reduced

(4) Long-term stable stage: in this stage, the maximum value of cumulative roof subsidence was 4.2 mm in the middle of the face, accounting for approximately 1% of the cumulative roof subsidence. This stable trend can be observed from the curve in Figure 17

5. Discussion

In general, the design of the ultimate technique for CCGPB was based on the mechanical properties, especially the unconfined uniaxial compressive strength (UCS) of the CCGPB samples prepared in the laboratory using conventional plastic molds. In addition, under standard maintenance conditions (GB/T50081-2002 by the concrete association in China), the temperature and humidity of the curing chamber were 20 ± 2 and 95% RH, respectively, and the curing duration was 28 days. However, some studies showed that laboratory studies are not particularly representative of the placement and curing conditions in underground mines. Some studies have shown that for a given

CCGPB technique and fixed curing duration, the *in situ* strengths of the CCGPB in noncoal mines were 2–4 times higher than those obtained in the laboratory [56–59]. These differences between the strength properties of CCGPB in mines and those in the laboratory can be partially explained by the effects of scaling on mixing, *in situ* placement, and curing conditions. For instance, the difference in the sizes of the stope mold can cause different CCGPB properties, such as the backfilling rate, stress state, strain rate, consolidation, arching, and shrinkage effects [60–65]. In particular, curing under an applied pressure caused an increase in the UCS of cemented soils and tailings [66]. In fact, it was challenging to determine the UCS properties of CCGPB in the field by laboratory test measures. The challenges included the selection of appropriate curing and placement conditions, such as the size and shape of the specimens for the laboratory tests [42, 67–69].

From the above monitoring results, it can be inferred that it is difficult to mimic the curing and placement conditions in the longwall backfilling working face of the coal mine. For coal mines with the commonly used Type U ventilation mode, the temperature and humidity of the working face were changeable at the different work sites. In addition, the placement condition was difficult to mimic because the roof stress applied on the paste backfill changed over time. The internal hydration temperature of the paste backfill showed that the increase in paste strength mainly occurred in the early stage. At the end of the early stage, the strength reached approximately 70% of the ultimate strength [70]. However, due to the arch structure of the stratified rock mass, in the early stage, the roof stress applied on the paste backfill was very small, accounting for approximately 1–3% of the whole overlying strata. In addition, the paste backfill contained 3–5% bleeding water. The drained paste backfill could produce higher mechanical strength than the undrained paste backfill. This phenomenon occurred because the removal of the excessive water within the backfill could accelerate the hydration of the binder and thus increase the strength and stability of the CCGPB. In summary, all of these factors in the field are very difficult to mimic in the laboratory. Therefore, to design the technique for CCGPB and model the overall quality and behavior of CCGPB, the authors suggest that comparative analysis should be conducted between the results from the laboratory-prepared sample tests and the field coring.

6. Conclusions

In this paper, field monitoring analysis was conducted on the curing and stress environment of CCGPB in an underground coal mine. The main results are summarized as follows:

(1) Temperature and humidity have a significant impact on the mechanical behavior and strength of CCGPB. The temperature was between 26°C and 28°C in the upper face, between 29°C and 32°C in the middle, and between 34°C and 37°C in the lower face. The humidity had the same change pattern as the temperature. The higher curing temperatures and humidity caused by the hydration reaction (up to 37°C and 81 RH) were advantageous for improving the rate of cement hydration and self-desiccation

(2) Based on the internal hydration temperature, the development of paste slurry can be divided into four stages, i.e., the rapid hydration stage, slower hydration stage, rapid decline stage, and relatively stable stage

(3) The trend of the applied roof loading (stress) on the backfill can be divided into five stages, i.e., the development stage, regulation stage, rapid growth stage, relatively stable stage, and long-term stable stage

(4) The roof subsidence trend can be divided into four stages, i.e., the rapid subsidence stage, slow subsidence stage, relatively stable stage, and long-term stable stage. The maximum roof subsidence was 104.3 mm in the middle and 90.2 mm on both sides

Data Availability

The data used to support the findings of this study are available from the corresponding author upon request.

Conflicts of Interest

The authors declare that there are no conflicts of interest in connection with the work submitted.

Authors' Contributions

Zhang Xinguo proposed the idea and drafted the manuscript; Zhao Jinhai analyzed the ingredients of CCGPB, conducted the indoor rock testing, and prepared the manuscript; Xin Lin conducted the indoor rock testing; Wang Kun and Pan Haiyang analyzed the experimental data.

Acknowledgments

Funding was provided by the Shandong Province Natural Science Foundation Project (ZR2017MEE055, ZR2020QE128, and 2018GSF116002); National Key R&D Program of China (2018YFC0604705); SDUST Research Fund (grant 2018TDJH102); National Natural Science Foundation of China (Grant nos. 51574159, 51974172, 51974173, and 51804179), and the SDUST Research Fund, China Postdoctoral Science Foundation (2015M572067 and 2016T90662).

References

[1] J. Zhao, J. Chen, X. Zhang, J. Ning, and Y. Zhang, "Distribution characteristics of floor pore water pressure based on similarity simulation experiments," *Bulletin of Engineering Geology and the Environment*, vol. 79, no. 9, pp. 4805–4816, 2020.

[2] T. Chen, J. H. Zhao, S. C. Zhang, Y. Zhang, F. Yang, and M. Li, "An experimental and analytical research on the evolution of mining cracks in deep floor rock mass," *Pure and Applied Geophysics*, vol. 177, no. 11, pp. 5325–5348, 2020.

[3] D. Wu, Y. Zhang, and C. Wang, "Modeling the thermal response of hydrating cemented gangue backfill with admixture of fly ash," *Thermochimica Acta*, vol. 623, pp. 86–94, 2016.
[4] D. Wu, G. Sun, and Y. Liu, "Modeling the thermo-hydro-chemical behavior of cemented coal gangue-fly ash backfill," *Construction & Building Materials*, vol. 111, pp. 522–528, 2016.
[5] D. Wu, Y. Hou, T. Deng, Y. Chen, and X. Zhao, "Thermal, hydraulic and mechanical performances of cemented coal gangue-fly ash backfill," *International Journal of Mineral Processing*, vol. 162, pp. 12–18, 2017.
[6] H.-q. ZhangLiu, "Mine green mining," *Energy Procedia*, vol. 16, pp. 409–416, 2012.
[7] D. Shang, G. Yin, X. Li et al., "Analysis for Green Mine (phosphate) performance of China: an evaluation index system," *Resources Policy*, vol. 46, pp. 71–84, 2015.
[8] C. Wang, Y. Lu, B. Shen, Y. Li, and Y. Liang, "Design and monitoring of CPB replacement mining RSCP: a case study in China," *Energy Sources Part A-Recovery Utilization and Environmental Effects*, vol. 43, 2021.
[9] L. Wang, M. Jiang, Y. Shen et al., "Distribution and evolution of residual voids in longwall old goaf," *Geomechanics and Engineering*, vol. 272, no. 2, pp. 121952–122114, 2019.
[10] B. E. Jimma and P. R. Rangaraju, "Film-forming ability of flowable cement pastes and its application in mixture proportioning of pervious concrete," *Construction and Building Materials*, vol. 71, pp. 273–282, 2014.
[11] A. Rafeet, R. Vinai, M. Soutsos, and W. Sha, "Guidelines for mix proportioning of fly ash/GGBS based alkali activated concretes," *Construction and Building Materials*, vol. 147, pp. 130–142, 2017.
[12] Z. Aldhafeeri, M. Fall, M. Pokharel, and Z. Pouramini, "Temperature dependence of the reactivity of cemented paste backfill," *Applied Geochemistry*, vol. 72, pp. 10–19, 2016.
[13] J. Frech-Baronet, L. Sorelli, and J. P. Charron, "New evidences on the effect of the internal relative humidity on the creep and relaxation behaviour of a cement paste by micro-indentation techniques," *Cement & Concrete Research*, vol. 91, 2017.
[14] L. Liu, X. Wang, H. Chen, and C. Wan, "Microstructure-based modelling of drying shrinkage and microcracking of cement paste at high relative humidity," *Construction and Building Materials*, vol. 126, pp. 410–425, 2016.
[15] A. Salem and S. Jamshidi, "Effect of paste humidity on kinetics of carbothermal reduction of extruded barite and coke mixture," *Solid State Sciences*, vol. 14, no. 8, pp. 1012–1017, 2012.
[16] S. Yilmaz, A. Belem, K. Bussière, Y. Mbonimpa, and Y. Benzaazoua, "Curing time effect on consolidation behaviour of cemented paste backfill containing different cement types and contents," *Construction & Building Materials*, vol. 75, no. 75, pp. 99–66, 2015.
[17] S. Cao and W. Song, "Effect of filling interval time on the mechanical strength and ultrasonic properties of cemented coarse tailing backfill," *International Journal of Mineral Processing*, vol. 166, 2017.
[18] J. Yilmaz, Q. Belem, and A. J. Benzaazoua, "Specimen size effect on strength behavior of cemented paste backfills subjected to different placement conditions," *Engineering Geology*, vol. 185, pp. 52–62, 2015.
[19] S. Yin, A. Wu, K. Hu, Y. Wang, and Y. Zhang, "The effect of solid components on the rheological and mechanical properties of cemented paste backfill," *Minerals Engineering*, vol. 35, no. 6, pp. 61–66, 2012.
[20] B. Ercikdi, A. Kesimal, F. Cihangir, H. Deveci, and İ. Alp, "Cemented paste backfill of sulphide-rich tailings: importance of binder type and dosage," *Cement and Concrete Composites*, vol. 31, no. 4, pp. 268–274, 2009.
[21] F. Cihangir, B. Ercikdi, A. Kesimal, A. Turan, and H. Deveci, "Utilisation of alkali-activated blast furnace slag in paste backfill of high-sulphide mill tailings: effect of binder type and dosage," *Minerals Engineering*, vol. 30, no. 4, pp. 33–43, 2012.
[22] S. LiHao, B. Bussière, M. Aubertin, and M. Benzaazoua, "Microstructural evolution of cemented paste backfill: mercury intrusion porosimetry test results," *Cement and Concrete Research*, vol. 37, no. 12, pp. 1654–1665, 2007.
[23] X. Yilmaz, J. Belem, J. Bussière, and F. Benzaazoua, "Relationships between microstructural properties and compressive strength of consolidated and unconsolidated cemented paste backfills," *Cement & Concrete Composites*, vol. 33, no. 6, p. 702, 2011.
[24] E. Wu, T. Deng, B. Liu, M. Liu, M. Chen, and F. Zha, "Strength and micro-structure evolution of compacted soils modified by admixtures of cement and metakaolin," *Construction and Building Materials*, vol. 127-128, pp. 44–51, 2016.
[25] C. Liang and M. Fall, "Mechanical and thermal properties of cemented tailings materials at early ages: influence of initial temperature, curing stress and drainage conditions," *Construction & Building Materials*, vol. 125, pp. 553–563, 2016.
[26] R. Le and C. Lassonde, *Comparison of the Material Properties of in Situ and Laboratory Prepared Cemented Paste Backfill*, ResearchGate, Berlin, Germany, 2002.
[27] T. Belem, M. Benzaazoua, B. Bussière, and A. M. Dagenais, *Effects of Settlement and Drainage on Strength Development within Mine Paste Backfill*, ResearchGate, Berlin, Germany, 2002.
[28] B. D. Thompson, W. F. Bawden, and M. W. Grabinsky, "In situ measurements of cemented paste backfill at the Cayeli Mine," *Canadian Geotechnical Journal*, vol. 49, no. 7, pp. 755–772, 2012.
[29] J. P. Doherty, A. Hasan, and G. H. Suazo, "An investigation of some controllable factors that impact the stress state in cemented paste backfill," *Canadian Geotechnical Journal*, vol. 52, no. 12, 2015.
[30] X. Wang, *Using Effective Stress Theory to Characterize the Behaviour of Backfill*, Vol. 100, Canadian Institute of Mining, Montreal, Canada, 2007.
[31] J. Zhang, L. Zhang, W. Spearing, X. Miao, S. Guo, and Q. Sun, "Stress-seepage coupling of cataclastic rock masses based on digital image technologies," *International Journal of Mining Science and Technology*, vol. 27, no. 1, pp. 17–27, 2017.
[32] J. Zhang, J. Lin, T. Liu, J. Song, and Y. Zhang, "Assessing the effectiveness of a high-temperature-programmed experimental system for simulating the spontaneous combustion properties of bituminous coal through thermokinetic analysis of four oxidation stages," *Energies*, vol. 169, no. 9, 2019.
[33] X. ZengShu and S. Zhang, "Experimental investigation on mechanical properties of in situ Cemented paste backfill containing coal gangue and fly ash," *Advances in Civil Engineering*, vol. 2020, Article ID 7964267, 12 pages, 2020.
[34] J. Zhao, X. Yin, N. Guo, and W. Guo, "Stress–seepage coupling of cataclastic rock masses based on digital image technologies," *Rock Mechanics and Rock Engineering*, vol. 79, no. 5, pp. 2529–2372, 2018.
[35] J. Zhao, N. Jiang, L. Yin, and B. Li-yang, "The effects of mining subsidence and drainage improvements on a waterlogged area," *Bulletin of Engineering Geology and the Environment*, vol. 78, no. 5, pp. 3815–3831, 2019.

[36] C. Lei, J. Deng, K. Cao et al., "A comparison of random forest and support vector machine approaches to predict coal spontaneous combustion in gob," *Fuel*, vol. 239, pp. 297–311, 2019.

[37] T. Yin, Y. Deng, and Z. Wang, "Assessing the effectiveness of a high-temperature-programmed experimental system for simulating the spontaneous combustion properties of bituminous coal through thermokinetic analysis of four oxidation stage," *Energy*, vol. 169, pp. 587–596, 2018.

[38] P. Shan, X. Lai, and X. M. Liu, "An associated evaluation methodology of initial stress level of coal-rock masses in steeply inclined coal seams, Urumchi coal field, China," *Engineering Computations*, vol. 37, no. 6, p. 2177, 2020.

[39] J. Zhao, X. Zhang, N. Jiang et al., "Porosity zoning characteristics of fault floor under fluid-solid coupling," *Bulletin of Engineering Geology and the Environment*, vol. 79, 2020.

[40] S. Chen, Z. Du, Z. Zhang, H. Zhang, Z. Xia, and F. Feng, "Effects of chloride on the early mechanical properties and microstructure of gangue-cemented paste backfill," *Construction and Building Materials*, vol. 235, p. 117504, 2020.

[41] S. Chen, Z. Du, Z. Zhang, D. Yin, F. Feng, and J. Ma, "Effects of red mud additions on gangue-cemented paste backfill properties," *Powder Technology*, vol. 367, pp. 833–840, 2020.

[42] L. Wang, M. Jin, F. Guo, W. Yan, and S. Tang, "Pore structural and fractal analysis of the influence of fly ash and silica fume on the mechanical property and abrasionresistance of concrete," *Fractals*, 2021.

[43] T. Zhao, Y. Zhang, Z. Zhang, Z. Li, and S. Ma, "Deformation monitoring of waste-rock-backfilled mining gob for ground control," *Sensors*, vol. 17, no. 5, pp. 1044–1056, 2017.

[44] C. Jiang, B. Niu, G. Yin, D. Zhang, T. Yu, and P. Wang, "CT-based 3D reconstruction of the geometry and propagation of hydraulic fracturing in shale," *Journal of Petroleum Science and Engineering*, vol. 179, pp. 899–911, 2019.

[45] Q. Liu, J. Chai, S. Chen, D. Zhang, Q. Yuan, and S. Wang, "Monitoring and correction of the stress in an anchor bolt based on pulse PrePumped brillouin optical time domain analysis," *Energy Science & Engineering*, vol. 8, no. 10, pp. 1–13, 2020.

[46] B.-y. Jiang, S.-t. Gu, L.-g. Wang, G.-c. Zhang, and W.-s. Li, "Strainburst process of marble in tunnel-excavation-induced stress path considering intermediate principal stress," *Journal of Central South University*, vol. 26, no. 4, pp. 984–999, 2019.

[47] X. T. Wang, S. C. Li, Z. H. Xu, J. Hu, D. D. Pan, and Y. G. Xue, "Risk assessment of water inrush in karst tunnels excavation based on normal cloud model," *Bulletin of Engineering Geology and the Environment*, vol. 78, pp. 3783–3798, 2019.

[48] E. Xu, T. Huang, M. Li, P. Lin, X. S. Shi, and J. Wu, "A new slice-based method for calculating the minimum safe thickness for a filled-type karst cave," *Bulletin of Engineering Geology and the Environment*, vol. 1–15, 2019.

[49] C. Wang, B. Shen, J. Chen et al., "Compression characteristics of filling gangue and simulation of mining with gangue backfilling: an experimental investigation," *Geomechanics and Engineering*, vol. 20, no. 6, pp. 485–495, 2020.

[50] N. Jiang, C. Wang, H. Pan, D. Yin, and J. Ma, "Modeling study on the influence of the strip filling mining sequence on mining-induced failure," *Energy Science & Engineering*, vol. 8, pp. 1–17, 2020.

[51] Z. Luo, R. Li, T. Wang et al., "Explosion pressure and flame characteristics of CO/CH4/air mixtures at elevated initial temperatures," *Fuel*, vol. 268, p. 117377, 2020.

[52] Z. Cheng, F. Cheng, and J. Deng, "Experimental study on the deflagration characteristics of methane-ethane mixtures in a closed duct," *Fuel*, vol. 259, p. 116295, 2020.

[53] B. Su, Z. Luo, T. Wang, K. Yan, F. Cheng, and J. Deng, "Coupling analysis of the flame emission spectra and explosion characteristics of CH4/C2H6/air mixtures," *Energy & Fuels*, vol. 34, 2020.

[54] J. Guo, H. Wen, X. Zheng, Y. Liu, and X. Cheng, "A method for evaluating the spontaneous combustion of coal by monitoring various gases," *Process Safety and Environmental Protection*, vol. 126, pp. 223–231, 2019.

[55] F. Cui, T. Zhang, X. Lai, J. Cao, and P. Shan, "Study on the evolution law of overburden breaking angle under repeated mining and the application of roof pressure relief," *Energies*, vol. 12, no. 23, pp. 4513–4532, 2019.

[56] A. Fourie, M. Helinski, and M. Fahey, *Filling the Gap-A Geomechanics Perspective*, University of Western Australia, Perth, Australia, 2006.

[57] B. Tikou, O. El Aatar, M. Benzaazoua, B. Bussière, and E. Yilmaz, *Hydro-geotechnical and Geochemical Characterization of Column Consolidated Cemented Paste Backfill*, Springer, Berlin, Germany, 2007.

[58] M. W. Grabinsky and W. Bawden, *Situ Measurements for Geomechanical Design of Cemented Paste Backfill Systems,* ResearchGate, Berlin, Germany, 2007.

[59] L. Wang, F. Guo, H. Yang, Y. Wang, and S. Tang, "Comparison of fly ash, PVA fiber, MgO and shrinkage-reducing admixture on the frost resistance of face slab concrete via pore structural and fractal analysis," *Fractals*, vol. 29, no. 2, Article ID 2140002, 2021.

[60] L. Li, M. Aubertin, and B. Tikou, "Erratum: formulation of a three dimensional analytical solution to evaluate stresses in backfilled vertical narrow openings," *Canadian Geotechnical Journal*, vol. 43, 2011.

[61] M. Helinski, M. Fahey, and A. Fourie, "Numerical modeling of cemented mine backfill deposition," *Journal of Geotechnical and Geoenvironmental Engineering*, vol. 133, 2007.

[62] M. Fahey, M. Helinski, and A. Fourie, "Some aspects of the mechanics of arching in backfilled stopes," *Canadian Geotechnical Journal*, vol. 46, 2009.

[63] B. Tikou, M. Benzaazoua, O. El Aaatar, and E. Yilmaz, "Effect of drainage and the pore water pressure dissipation on the backfilling sequencing," in *Proceedings of the 23rd World Mining Congress*, Montréal, Canada, August 2013.

[64] F. Chen, S. Lu, X. Ding, and Y. Ju, "Evaluation of the density and thickness of adsorbed methane in differently sized pores contributed by various components in a shale gas reservoir: a case study of the Longmaxi Shale in Southeast Chongqing, China," *Chemical Engineering Journal*, vol. 367, pp. 123–138, 2019.

[65] F. Chen, H. Zhao, S. Lu, X. Ding, and Y. Ju, "The effects of composition, laminar structure and burial depth on connected pore characteristics in a shale oil reservoir, the Raoyang Sag of the Bohai Bay Basin, China," *Marine and Petroleum Geology*, vol. 101, pp. 290–302, 2019.

[66] N. Consoli, V. Rotta G, and P. Prietto, "Yielding-compressibility-strength relationship for an artificially cemented soil cured under stress," *Geotechnique*, vol. 56, 2006.

[67] F. Zhou, W. B. Sun, J. L. Shao, L. J. Kong, and X. Y. Geng, "Experimental study on nano silica modified cement base grouting reinforcement materials," *Geomechanics and Engineering*, vol. 20, no. 1, pp. 67–73, 2020.

[68] E. Xue, T. Sun, and M. Wu, "The influence of magmatic rock thickness on fracture and instability law of mining surrounding rock," *Cement and Concrete Composites*, vol. 20, 2020.

[69] W. Sun and F. Zhou, "Experimental study on Portland cement/calcium sulfoaluminate binder of paste filling," *European Journal of Environmental and Civil Engineering*, 2020.
[70] L. Wang, M. Jin, Y. Wu, Y. Zhou, and S. Tang, "Hydration, shrinkage, pore structure and fractal dimension of silica fume modified low heat Portland cement-based materials," *Construction and Building Materials*, vol. 2021, p. 272, 2021.